Journal of Magnetism and Magnetic Materials 584 (2023) 171072

Contents lists available at ScienceDirect

Journal of Magnetism and Magnetic Materials

journal homepage: www.elsevier.com/locate/jmmm

Concentration transition in $Cu_2(Mn,Ga)BO_5$ solid solutions

Evgeniya Moshkina [a,*], Evgeniy Eremin [a,b], Alexey Veligzhanin [c], Maksim Pavlovskiy [a], Svetlana Sofronova [a], Veronika Titova [a], Leonard Bezmaternykh [a]

[a] Kirensky Institute of Physics, Federal Research Center KSC SB RAS, Krasnoyarsk 660036, Russia
[b] Siberian State University of Science and Technologies, Krasnoyarsk 660037, Russia
[c] National Research Centre "Kurchatov Institute", Moscow 123182, Russia

ARTICLE INFO

Keywords:
Ludwigite
Solid solution
Magnetic phase transition
Spin glass state

ABSTRACT

The effects related to the conversion of magnetic structures of a Cu_2MnBO_5 ferrimagnet to a Cu_2GaBO_5 antiferromagnet under the $Mn^{3+} \rightarrow Ga^{3+}$ substitution were studied. The properties of four single crystal samples with the gallium concentration $x = 0.04, 0.11, 0.17, 0.25$ were examined. The chemical composition and valence state of the samples were determined by X-ray absorption spectroscopy element-sensitive technique. Distribution of the 3*d* metal ions over crystallographic positions was studied using the first principle calculations by Wien2k program. The evolution of the magnetic properties was investigated by the measurements of the temperature and field dependences of magnetization, *dc* and *ac* magnetic susceptibility. In agreement with the previous study of the structure evolution of $Cu_2Mn_{1-x}Ga_xBO_5$ solid solutions, the critical concentration upon a change in the magnetic ordering type was found in the range $x = 0.17$–0.25. The non-monotonic behavior of magnetization in terms of the gallium content was found in the concentration range of 0.04–0.17. A complex pattern of magnetic phase transitions belonging to the concentration phase boundary was obtained in the compounds with gallium being within the range $x = 0.17$–0.25. One could observe the splitting of the peaks of the real part of *ac*-susceptibility of the high-temperature phase transition in the Cu_2MnBO_5-like phase ($x = 0.04, 0.11$) and that of the low-temperature one at the concentration boundary ($x = 0.17, 0.25$) with different frequency and orientational dependence. The type and origin of the multiple phase transitions observed in the studied samples were analyzed.

1. Introduction

Cu_2MnBO_5 possesses a unique crystal structure among both orthorhombic (natural) and Cu-containing monoclinic ludwigites: it is monoclinic but characterized by another direction of the monoclinic axis and other distortions of Me-O octahedra [1,2]. This structural peculiarity is likely to be related to the simultaneous presence of two Jahn-Teller ions, Cu^{2+} and Mn^{3+}. In terms of magnetic properties, Cu_2MnBO_5 is a ferrimagnet below $T_C = 92$ K and its non-collinear magnetic structure consists of two antiferromagnetic subsystems, the angle between the axes of these subsystems being about 60° [3].

The substitution of the $Mn^{3+} \rightarrow Ga^{3+}$ type in the concentration range from 32 up to 47 at. % (according to EDX data (energy dispersive X-ray spectroscopy)) resulted in the Cu_2GaBO_5-type structure in solid solutions. Cu_2GaBO_5 is an antiferromagnet below $T_N = 4.1$ K with 50% paramagnetic cation positions: there is ordering in one of the subsystems containing only copper [4]. Since Cu_2GaBO_5 possesses the classic structure of monoclinic ludwigite, a concentration-driven phase transition is expected in a series of solid solutions Cu_2MnBO_5 - Cu_2GaBO_5 with the corresponding magnetic restructuring. The magnetic properties of $Cu_2(Mn,Ga)BO_5$ solid solutions with the 32–47 at. % gallium substitution are similar to parent Cu_2GaBO_5. However, antiferromagnetic ordering is here accompanied by the spin glass phase, caused by magnetic Mn^{3+} being admixed to the mixed Ga^{3+} and Cu^{2+} positions, which earlier did not participate in the magnetic ordering [5].

In [6], $Cu_2(Mn,Ga)BO_5$ solid solutions were obtained in the gallium substitution range of 3–25 at. % (according to EDX data) with the purpose of detecting and studying the concentration phase transition. The cation composition and structure of the samples were investigated by the X-ray diffraction (single crystal and powder) and vibrational (Raman) spectroscopy. The concentration-driven phase transition was found in the range of 18.7–25 at. % of gallium. The X-ray diffraction

* Corresponding author.
E-mail address: ekoles@iph.krasn.ru (E. Moshkina).

https://doi.org/10.1016/j.jmmm.2023.171072
Received 6 April 2023; Received in revised form 19 July 2023; Accepted 24 July 2023
Available online 26 July 2023

study revealed a change in the direction of the monoclinic axis between the concentrations 18.7 at. % and 25 at. %. The Raman spectroscopy showed a significant spectral difference from parent Cu_2MnBO_5 at the gallium concentration as low as 18.7 at. % [6].

This work continues the investigation of $Cu_2(Mn,Ga)BO_5$ solid solutions with high manganese content, including the study of the concentration phase boundary Cu_2MnBO_5 - Cu_2GaBO_5 in terms of the real chemical and valent composition by element selective techniques of X-ray absorption spectroscopy, position distribution by the first-principle calculation, and changes in the magnetic properties.

2. Experimental

2.1. X-ray absorption spectroscopy

The X-ray absorption spectra were measured in the transmission geometry at the "Structural material science" beamline at the Kurchatov source of synchrotron radiation [7]. The energy of x-rays was determined by a channel-cut Si (1 1 1) monochromator. The beam size of the synchrotron radiation on the sample was 1 × 3 mm^2 (V × H). The samples were prepared as tablets by pressing a finely ground sample with starch used as a binding agent. The amount of the sample was chosen so that the tablet absorption coefficient μt be no more than 3–3.5 in the entire energy range. The intensity of the incoming and transmitted X-rays was measured using ionization chambers filled with an air-argon mixture equipped with Keithley 6487 pikoammeters. The point by point measurements of the absorption spectra were carried out in the range −170 eV – +800 eV relative to the energy of *K*-edge absorption of the absorbing elements – manganese (6539 eV), copper (8979 eV) and gallium (10367 eV).

Each spectrum was measured for about 20 min. The spectral measurements of each sample were made 2–3 times and averaged. Processing and analysis of the results were performed using the Athena program from IFEFFIT software package (version 1.2.11c) [8–9].

The manganese and copper valence states were estimated by the "fingerprint" analysis of XANES spectra. For this purpose, a comparison was made of the position of *K*-edge absorption of manganese and copper in the studied sample with a set of standards: MnB_2O_4 (Mn^{2+}), Mn_2O_3 (Mn^{3+}), MnO_2 (Mn^{4+}), Cu_2O (Cu^{+}), CuO (Cu^{2+}), $CuCl_2{\cdot}2H_2O$ (Cu^{2+}), metallic Cu. The shape of *K*-absorption edge of the samples and the first derivative of the absorption spectra were visually analyzed to determine the positions of the inflection points, related to the valence state of the absorbing atom.

2.2. First-principle calculation

The energy calculation of different cationic ordered states of Cu_2MnBO_5 and Cu_2GaBO_5 was made in the framework of the first principle approach using the Wien2K program package [10–11]. There are twelve metal ions in the unit cell of ludwigite. Based on the electro neutrality, four metal ions have to be trivalent (these ions are supposed to be manganese and gallium) and eight of them are bivalent (copper ions). In most ludwigites trivalent ions prefer to occupy position 4. The energy of this cationic ordered state was chosen as a reference point (E_0) and all the other energies were compared to this one. The calculation was performed for the nonmagnetic state. The electronic structure was calculated using the FP-LAPW + lo method [12]. The exchange–correlation energy was calculated using LSDA [13] and GGA-PBE [14] with additional correlation Hubbard coefficients describing local electron–electron repulsion related to the 3d-zones of Cu and Mn (LSDA + U and GGA-PBE + U) [15]. The experimental lattice parameters and atomic coordinates were used for the calculation. The value of $R_{MT}{*}K_{max}$ was equal to 6.0 in the calculation. The energy upon the self-consistent calculation was converged within 1 μRy. The total energy was reduced to minimum using a set of 400 *k*-points in the full Brillouin zone of the unit cell. The radii of the MT-spheres were 1.93 atomic units for Cu, 1.86 atomic units for Ga, 1.08 atomic units for B and 1.1 atomic units for O. The total density of the states (DOS) was obtained using the modified Blech tetrahedra method [16]. Here, U = 0.52 Ry was used for Cu and Ga, U = 2.52 Ry for Mn and $J = 0Ry$ in the schemes LSDA + U and GGA-PBE + U.

2.3. Laue technique

The single crystals under study were oriented using a Photonic Science Laue Crystal Orientation System by the back reflection method with an X-ray beam diameter of 0.2 mm. For all the samples, the diffraction pattern obtained upon the reflection of the primary beam from the natural face of the crystal was found to correspond to the plane with indices (0 1 1). The lattice vector *a* was directed along the long edge of the natural face. To assess the quality of the single crystals under study, a series of diffraction patterns was taken at different points of the natural (0 1 1) face of each sample by gradually moving the crystal relative to the beam with a step of 0.2 mm (the accuracy of the goniometer was 0.001 mm).

For the samples with $x = 0.05$, 0.1 and 0.175 (flux gallium concentration), all the obtained Laue patterns corresponded to the reflection plane (0 1 1) and to the given lattice parameters (for $x = 0.175$, the lattice parameters used: $a = 3.167$ Å, $b = 11.995$ Å, $c = 9.406$ Å, $\beta = 96.23°$), with no splitting and blurring of the reflections being observed. No additional peaks which could indicate the presence of the second phase were observed. Thus, the above allowed us to conclude that the quality of the single crystals was good ($x = 0.05$, 0.1 and 0.175).

For the sample with $x = 0.15$, the resulting Laue patterns showed the splitting of the peaks, including the central one, which may indicate the presence of misoriented domains in the sample.

2.4. Magnetic measurements

Temperature-field magnetization dependences and temperature dependences of *ac*-susceptibility of the synthesized samples were obtained in the temperature range of 4.2–300 K and in the magnetic fields up to 9 T using PPMS-9 (Quantum Design). The thermal dependences of magnetization of the $Cu_2(Mn, Ga)BO_5$ solid solutions were measured at a magnetic field $H = 200$ Oe in the FC mode (sample cooling in a non-zero magnetic field), FH mode (sample heating in a non-zero magnetic field after cooling in the magnetic field of the same value) and ZFC mode (sample heating in a non-zero magnetic field after cooling in a zero magnetic field). The measurements were made upon applying the magnetic field along three mutually perpendicular directions (*x*, *y*, *z*) corresponding to macroscopic directions of the natural crystal habit which represents elongated four-cornered prisms with truncated side ribs. The directions (*x*, *y*, *z*) correspond to the following crystallographic directions: $x||n_{011}$ (normal to the (0 1 1) plane), $y\perp(x,z)$, $z||a$ (Fig. 1).

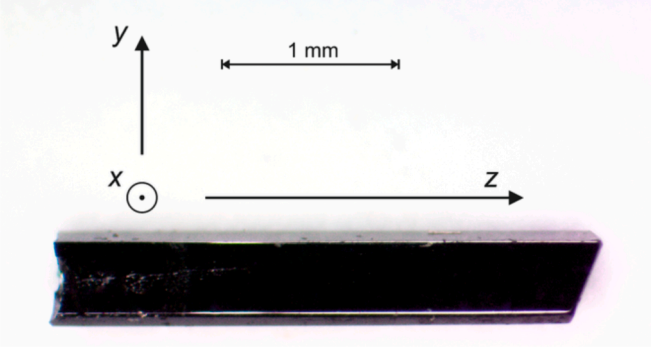

Fig. 1. The grown single crystal of $Cu_2Mn_{1-x}Ga_xBO_5$ (at $x = 0.1$ – flux concentration) and designation of the axes (*x*, *y*, *z*) directions along which the magnetic field was applied.

3. Chemical and valence composition and cation distribution

The composition of the studied samples was estimated via the height of the absorption jumps by the X-ray absorption spectroscopy. The results are presented in Table 1. The heights of the absorption jumps for the edges of Mn, Cu and Ga were determined by the measurements the absorption spectra through all three edges at the same tablet to ensure the equal thickness of the sample. In this case the relative content of the cations was determined by formula:

$$c_i \propto \frac{w_i}{M_i} \propto \frac{(\Delta_i \mu t)_{\exp}}{M_i \cdot \Delta(\mu/\rho)_i}; \quad (1)$$

where i corresponds to absorbing atom, c — atomic concentration, w — weight concentration, M — molar mass, $\Delta\mu t$ — measured height of the absorption jump, $\Delta(\mu/\rho)$ — change in mass attenuation coefficient at the absorption edge [17].

The measured XANES spectra at manganese and copper K-edges are shown at Fig. 2 with their derivative. The positions of experimental spectra of K-edge absorption of manganese agree well with standard Mn_2O_3, where manganese is in the trivalent state. However, there is a tiny shift to lower energies can be seen, indicating the presence of small amount of Mn^{2+}. The shift of the broad peak in the derivative, showing the position of the inflection point in the spectrum, to the lower energies can be seen as well. The positions of spectra at copper K-edge coincide for all samples and situated close to that for divalent copper standards -$CuCl_2 \cdot 2H_2O$ and CuO. The difference can be attributed to the influence of local environment of copper in the samples which differs from that of the standards.

As one can see from Table 1, the experimentally estimated gallium content in the samples is quite close to the flux concentration (x_{flux}) for the samples of the Cu_2MnBO_5-type phase. For the sample of the Cu_2GaBO_5-type phase the data of X-ray absorption spectroscopy and EDX show a significant deviation of the actual composition from that in the flux (25% instead of 17.5%). Here, the experimental data are in good agreement. The copper content in each sample is lower than 2/3, allowing to estimate the amount of bivalent manganese from 0.09 to 0.2 of atoms in the formula based on the electroneutrality.

The first-principle calculation of the energy of the Cu_2MnBO_5 and Cu_2GaBO_5 ludwigites, depending on the occupation of four nonequivalent cation sites of the unit cell, was made for the theoretical study of the cation distribution. The difference between the total energy of the compound with the arrangement of the trivalent ions in different crystallographic positions and the total energy of the compound when all the trivalent ions are located in position 4 is presented in Tables 2 and 3.

As one can see from Table 2, trivalent manganese cations prefer to occupy position 4. The displacement of Mn ions to another position is not equally beneficial for all the crystallographic positions. This ion distribution is in good agreement with the experimental data obtained by neutron diffraction [3].

In Cu_2GaBO_5, on the contrary, trivalent gallium tends to partially occupy position 4. The minimum energy was obtained for the compound where position 1 was fully occupied by gallium, position 2 was occupied by one gallium ion and one copper ion. In addition, one gallium ion is located in position 4. As one can see from Table 3, gallium ions tend to occupy positions 1 and 2, and, partially, position 4. However, the occupation of position 3 is not beneficial at all, which is consistent with the experimental data: trivalent gallium cations are distributed over nonequivalent positions in the ludwigite unit cell.

4. Magnetic properties

The temperature dependences of magnetization of the studied samples are presented in Fig. 3. The analogous dependences of the parent Cu_2MnBO_5 ludwigite are also shown for comparison. As is shown earlier [3], below the temperature of magnetic phase transition $T_C = 92$ K, Cu_2MnBO_5 demonstrates a rather strong temperature hysteresis of the FC-FH dependences and inflection of the ZFC curve. This, to a high extent, depends on the value of the applied magnetic field: the effect was observed in the field up to 500 Oe, while in the magnetic field $H = 1$ kOe the hysteresis was absent. Upon increasing the magnetic field, the temperature of this feature decreases. The origin of the observed thermal hysteresis of the FC-FH curves was not studied enough – it was characterized as a consequence of the reorientation of the "easy" magnetic axes in the crystal. Therefore, the orientational dependences were measured in the magnetic fields $H = 200$ Oe to study the evolution of the magnetic properties upon the Mn → Ga substitution, including this thermal hysteresis.

As one can see in Fig. 3 the thermal dependences of magnetization of the $Cu_2(Mn, Ga)BO_5$ solid solutions are anisotropic, which qualitatively corresponds to the behavior of pure Cu_2MnBO_5, including the magnetic fields with a larger value [2–3]. Upon increasing the $Mn^{3+} \rightarrow Ga^{3+}$ substitution degree the temperature of the magnetic phase transition decreases monotonically from $T_C = 92$ K to $T_C = 56$ K that typical at nonmagnetic ion replacement [18]. However, the value of the magnetic moment of the solid solutions with different substitution degree in the range of the occurrence of the Cu_2MnBO_5-like phase behaves rather nonmonotonically: the value of the magnetic moment of the sample with 0.04 of gallium is lower than that for the samples with 0.11 and 0.17 of gallium for each direction. The magnetic moment of the sample with 0.11 of gallium at $H||x$ is a quarter larger the magnetic moment of pure Cu_2MnBO_5, while in the direction $H||z$ it is almost equal to the latter. Such behavior describes the change in the cationic distribution over four nonequivalent positions. Since the magnetic structure of copper-manganese ludwigite contains two canted subsystems with the antiferromagnetic arrangement of the magnetic moments inside, and gallium cations tend to be located in two positions (one of them is Mn^{3+} position, another one is occupied by Cu^{2+}), the different substitution degree by nonmagnetic Ga^{3+} leads to a change in the values of magnetic moments in different sites of antiferromagnetically interacting subsystems, which is reflected in the exchange magnetic structure of the whole sample.

Fig. 3 shows the change in the thermal hysteresis loop of the FH-FC curves upon increasing the gallium content. The difference in the magnetization values tends to monotonically decrease in the curves. However, the temperature range of hysteresis is almost constant. This thermal hysteresis is present in the curves up to the critical concentration of the Cu_2MnBO_5-like phase stability ($x_C = 0.17$).

The transformation of the magnetic properties upon the change in the Cu_2MnBO_5 - Cu_2GaBO_5 phase resulting from the gradual substitution of Mn^{3+} by Ga^{3+} occurs in a narrow concentration range, as one can see

Table 1
The chemical composition of $Cu_2Mn_{1-x}Ga_xBO_5$ ludwigites obtained by spectroscopy of X-ray absorption (x_{XA}) (x_{flux} is the gallium concentration in the flux, x_{EDX} is the gallium concentration obtained by EDX [6]).

	$Cu_2Ga_{0.05}Mn_{0.95}BO_5$	$Cu_2Ga_{0.1}Mn_{0.9}BO_5$	$Cu_2Ga_{0.15}Mn_{0.85}BO_5$	$Cu_2Ga_{0.175}Mn_{0.825}BO_5$
Mn	38.6%	33.9%	30.6%	28.0%
Cu	60.0%	62.4%	63.8%	63.6%
Ga	1.4%	3.6%	5.6%	8.4%
x_{XA}	0.042	0.11	0.168	0.25
x_{flux}	0.05	0.10	0.15	0.175
x_{EDX}	0.023	0.088	0.187	0.25

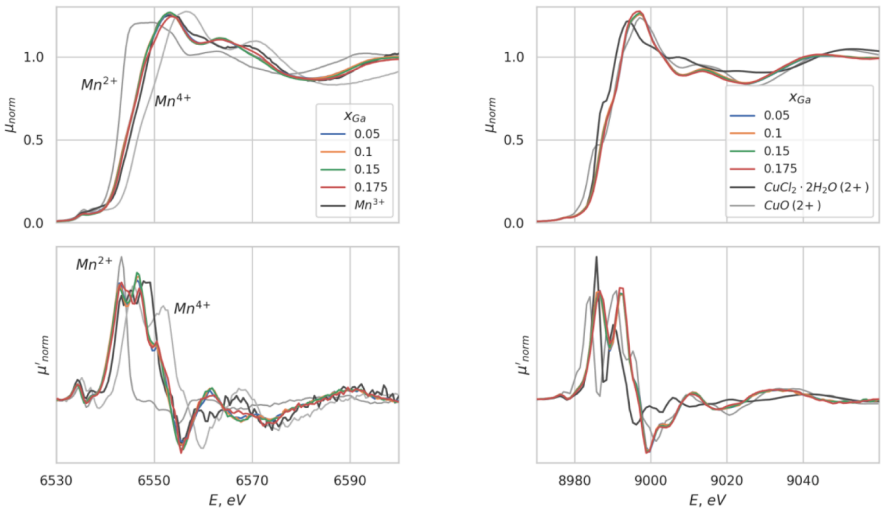

Fig. 2. The XANES spectra and it energy derivative for manganese K-edge (a) and copper K-edge (b). The spectra for the standards MnB_2O_4 (Mn^{2+}), Mn_2O_3 (Mn^{3+}), MnO_2 (Mn^{4+}), CuO (Cu^{2+}) and $CuCl_2{\cdot}2H_2O$ (Cu^{2+}) are also shown.

Table 2
The difference between the total energy at the location of copper cations in different crystallographic positions and the total energy upon the occupation of position 4 by trivalent ions only, for Cu_2MnBO_5.

1	2	3	4	ΔE
Cu,Cu	Cu,Cu	Cu,Cu,Cu,Cu	Mn,Mn,Mn,Mn	0
Cu,Cu	Cu,Cu	Cu,Cu,Cu,**Mn**	Mn,Mn,Mn,Cu	0.119943
Cu,Cu	Cu,**Mn**	Cu,Cu,Cu,Cu	Mn,Mn,Mn,Cu	0.120961
Cu,**Mn**	Cu,Cu	Cu,Cu,Cu,Cu	Mn,Mn,Mn,Cu	0.1148477

in Fig. 3. There occurs a rapid decrease in the magnetic moment with the gallium content $x = 0.17$. With this concentration one can observe the phase separation in the flux at the growth stage due to the high sensitivity of the magnetic properties of the studied solid solutions to a minor change in the Mn/Ga/Cu ratio and cation distribution. As is shown in the previous work [6], there is no polyphase in the samples of $Cu_2(Mn, Ga)BO_5$, which is in agreement with its structure and phase content studied using powder X-ray diffraction. The Raman spectroscopy study showed a significant difference in the spectra of the sample with this "critical" concentration and those of the parent Cu_2MnBO_5-like and Cu_2GaBO_5-like phases.

In agreement with the results of magnetic measurements, the samples with $x = 0.17$ can be divided into two phases: the Cu_2MnBO_5-like phase with one phase transition with a tiny FH-FC hysteresis and significant magnetization lowering relative to pure Cu_2MnBO_5, and the phase of the transition area with the subsequent decrease in magnetization and two phase transitions inherited from both parent Cu_2MnBO_5 and Cu_2GaBO_5 ludwigites (Fig. 3).The upper phase transition is characterized by the temperature $T_1 = 56$ K, and the lower one by $T_2 = 20$ K. Similar behavior of the $M(T)$ curves is observed in the sample with $x = 0.25$. However, this compound is isostructural to Cu_2GaBO_5 with a small deviation of the lattice parameters from the monotonic concentration dependence [6]. In these samples there occurs the growth of magnetization at $T_1 = 56$ K and a peak in the $M(T)$ curves at the temperatures about $T_2 = 20$ K. The thermal hysteresis of the FH-FC curves is absent in the sample with $x = 0.25$. However, in the area of the upper transition one can observe the region of inconsistency in the FC-ZFC curves obtained upon heating and cooling the sample, correspondingly. The phase homogeneity of the sample was confirmed by powder X-ray diffraction and Laue technique; the structure was verified in different points of the single crystal used for the magnetization measurements.

The thermal dependences of the partial derivatives $\partial M^2/\partial T(T)$were plotted for a more complete analysis of the $M(T)$ curves of the obtained $Cu_2(Mn,Ga)BO_5$ solid solutions. The $M^2(T)$ dependences are proportional to the magnetic contribution to the specific heat, which is in agreement with the molecular field theory [19]. This correspondence is valid for ferromagnets. Thus, the $\partial M^2/\partial T(T)$ dependences can be used for describing the ferrimagnetic phase transition occurring in the Cu_2MnBO_5-like phase. The obtained dependences are presented in Fig. 4. For antiferromagnets the magnetic contribution to the specific heat is proportional to $\chi{\cdot}T$ [20]. Thus, the $\partial(\chi T)/\partial T(T)$ dependences are

Table 3
The difference between the total energy at the location of copper cations in different crystallographic positions and the total energy upon the occupation of position 4 by trivalent ions only, for Cu_2GaBO_5.

	1 (2*b*)		2 (2*c*)		3 (4 *g*)				4 (4 *h*)				
0	Cu	Cu	Cu	Cu	Cu	Cu	Cu	Cu	Ga	Ga	Ga	Ga	0
1	Cu	Cu	Cu	Ga	Cu	Cu	Cu	Cu	Ga	Cu	Ga	Ga	−0.00178
2	Cu	Cu	Ga	Ga	Cu	Cu	Cu	Cu	Ga	Cu	Cu	Ga	−0.017558
3	Cu	Ga	Ga	Cu	Cu	Cu	Cu	Cu	Ga	Cu	Cu	Ga	−0.022136
4	Cu	Ga	Ga	Ga	Cu	Cu	Cu	Cu	Ga	Cu	Cu	Cu	−0.051471
5	Ga	Ga	Ga	Ga	Cu	Cu	Cu	Cu	Cu	Cu	Cu	Cu	−0.051437
6	Ga	Ga	Cu	Ga	Cu	Cu	Cu	Cu	Ga	Cu	Cu	Cu	−0.236291
7	Ga	Ga	Ga	Cu	Cu	Cu	Cu	Cu	Ga	Cu	Cu	Cu	−0.042455
8	Ga	Ga	Cu	Ga	Cu	Cu	Cu	Cu	Cu	Ga	Cu	Cu	−0.47253
9	Ga	Ga	Cu	Ga	Cu	Cu	Cu	Cu	Cu	Cu	Ga	Cu	−0.42454
10	Cu	Cu	Ga	Ga	Cu	Ga	Cu	Cu	Ga	Cu	Cu	Cu	0.152606

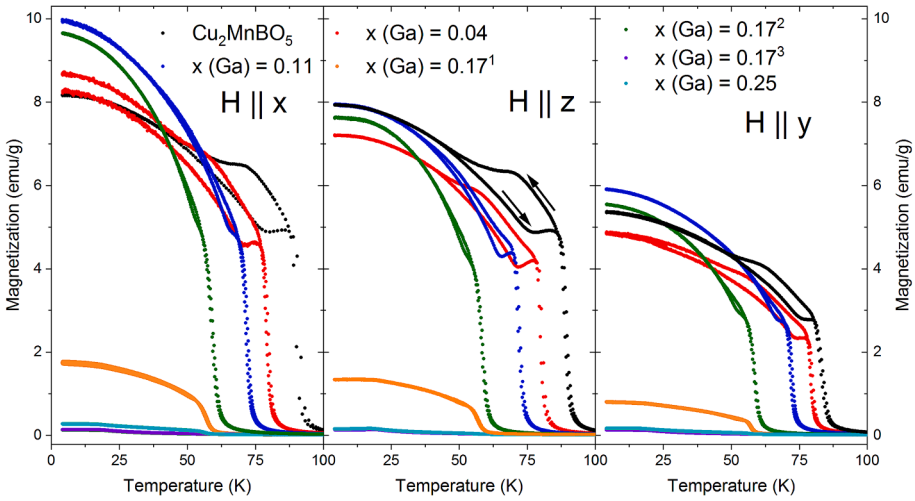

Fig. 3. The thermal dependences of magnetization of $Cu_2(Mn, Ga)BO_5$ solid solutions, obtained in the magnetic fields $H = 200$ Oe, in the $H||x$, $H||y$, $H||z$ in FC and FH modes (cooling in the magnetic field and heating in the magnetic field of the same value). Color indication: black - Cu_2MnBO_5 ($x = 0$), red - $x = 0.04$, blue - $x = 0.11$, orange - $x = 0.17^1$, green - $x = 0.17^2$, violet - $x = 0.17^{3,}$ cian - $x = 0.25$. The arrows in $H||z$ Cu_2MnBO_5 dependences show the way of temperature change: the top arrow indicates the FC mode (decreasing of the temperature), the bottom arrow indicates the FH mode (increasing of the temperature). This description is true for all the others curves.

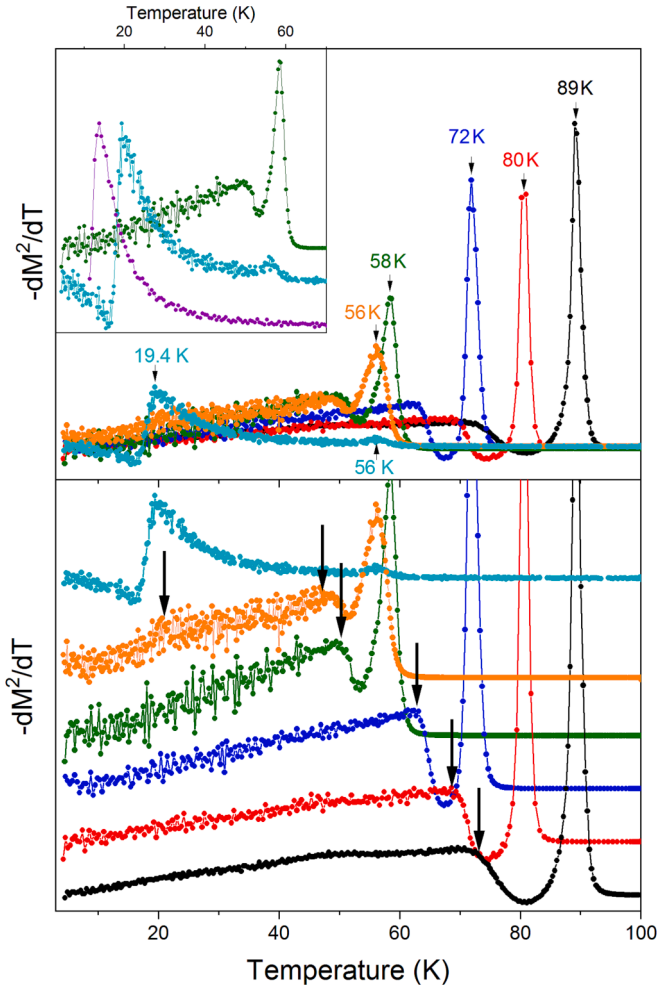

Fig. 4. The thermal dependences of the partial derivatives $\partial M^2/\partial T(T)$ of the obtained $Cu_2(Mn, Ga)BO_5$ solid solutions. The derivative was based on $M(T)$ dependence which was obtained at $H = 200$ Oe, in the direction $H||z$. a) the general view of $\partial M^2/\partial T(T)$ with the denoted phase transition temperatures; b) the detailed view of the low-intensity part of the derivatives with the peak identification corresponding to the $M(T)$ thermal hysteresis of the Cu_2MnBO_5-like phase; inset: the comparison of $\partial M^2/\partial T(T)$ at the critical concentrations $x = 0.17$, 0.25 and in the Cu_2GaBO_5-like phase (gallium concentration $x = 0.42$).

also present due to the antiferromagnetic origin of magnetic phase transition in another parent Cu_2GaBO_5 ludwigite (Fig. 5).

As one can see from Fig. 4, up to the critical concentration, the substituted compounds demonstrate quite an intensive and narrow peak corresponding to the ferrimagnetic phase transition and a broad low-temperature wing with the maximum related to the inflection of $M(T)$ in the range of FH-FC thermal hysteresis. As the gallium content increases, the temperatures of these maxima shift to the low-temperature area. One of the curves demonstrates three peaks on the boundary of the Cu_2MnBO_5-phase stability (at $x = 0.17$): two high-temperature ones are related to the ferrimagnetic phase transition and FH-FC hysteresis, while the third peak is the least intensive, corresponding to the phase transition inherited from the Cu_2GaBO_5-like phase. Upon lowering the ferrimagnetic phase transition temperature (T_1) and, hence, increasing the gallium concentration, T_1 peak intensity decreases rapidly, and the wing disappears, but the intensity of the low-temperature antiferromagnetic phase transition increases. With further increase in the gallium concentration the peak related to ferrimagnetic transition disappears. Hence, the concentration phase transition in the Cu_2MnBO_5-Cu_2GaBO_5 system occurs in some range of the critical concentrations with the gradual restructuring of the magnetic subsystems. There are some differences in peaks found on the $\partial M^2/\partial T(T)$ curves: the peaks related to ferrimagnetic transition are symmetrical ones; antiferromagnetic transition peaks are broad and asymmetrical ones with the typical inflection accompanied by the negative section of curves. Thus, it can be concluded that the analysis of the $\partial M^2/\partial T(T)$ curves is less appropriate for antiferromagnetic materials due to the ambiguous determination of the critical temperatures.

Ferrimagnetic and antiferromagnetic phase transitions in the $\partial(\chi T)/\partial T(T)$ curves are also manifested in different ways. Using such an analysis it is possible to divide phase transitions into types and classify them. The $\partial(\chi T)/\partial T(T)$ and $\chi T(T)$ curves of the studied solid solutions are presented in Fig. 5. The ZFC dependences, obtained at $H \perp z$, were taken as a source for plotting. Therefore, the curves contain anomalies related to the "defrosting" of magnetic moments – inflection in the temperature range of $T = 25$–30 K.

All the curves corresponding to the samples with $x = 0.04$–0.17 of gallium, presented in Fig. 5, behave in a similar way. However, the curves for $x = 0.17$ are different in the low-temperature part: there is a peak corresponding to phase transition inherited from Cu_2GaBO_5. The features of the $\partial(\chi T)/\partial T(T)$ dependences related to phase transition of the Cu_2MnBO_5-like phase are the negative peaks, while those related to the Cu_2GaBO_5-like phase are the positive ones. This demonstrates the difference in the origin of these phase transitions. There are weak negative peaks T_2 corresponding to the FH-FC thermal hysteresis along

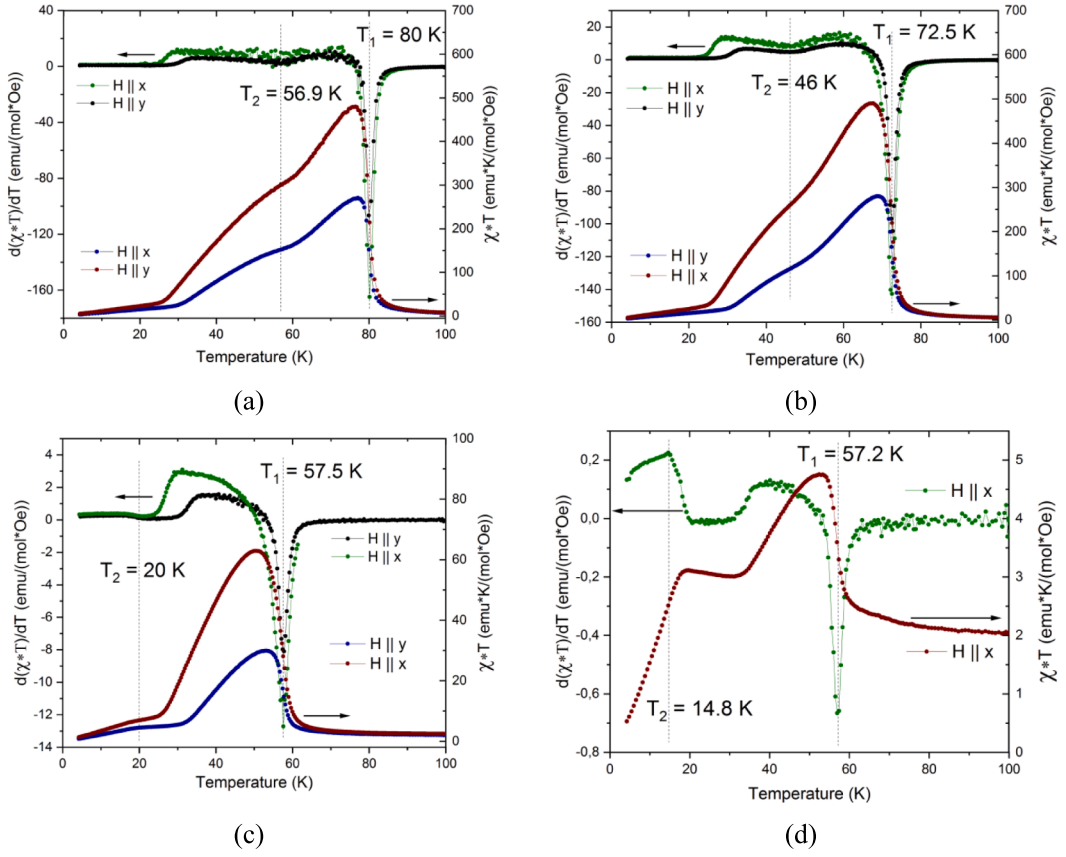

Fig. 5. The thermal dependences of $\partial(\chi T)/\partial T(T)$ and $\chi T(T)$ of the $Cu_2Mn_{1-x}Ga_xBO_5$ solid solutions with the high manganese concentration (a – 0.04, b – 0.11, c – 0.17, d – 0.25).

with the narrow intensive ferrimagnetic peaks of T_1 in the samples with lower gallium content (x = 0.04–0.11). In the sample with x = 0.17 there is no peak of FH-FC hysteresis in these dependences. Temperature T_2 denotes the antiferromagnetic phase transition corresponding to the beginning of the Cu_2GaBO_5-like phase. As one can see in Fig. 5 the sample with x = 0.25 demonstrates a significant difference from the samples with lower gallium content: the magnetic moment "defrosting" temperature is in the range of T = 30–40 K, there is a sharp negative peak T_1 = 57.2 K of ferrimagnetic transition and quite a pronounced broad maximum of antiferromagnetic one at low temperatures (T_2 = 14.8 K). Using this analysis, it was possible to clarify the temperatures of phase transitions realized in the studied samples and to divide them by the type.

Along with the thermal dependences of magnetization, the field dependences of magnetization of the solid solutions were obtained and analyzed at T = 4.2 K. Fig. 6 presents these dependences for several compositions of the $Cu_2Mn_{1-x}Ga_xBO_5$ solid solutions, obtained upon applying the magnetic field in the direction $H||z$. Despite the increase in the magnetic moment in the low field (Fig. 3, H = 200 Oe), outside the hysteresis loop under quite a strong magnetic field the magnetization of Cu_2MnBO_5 is higher than the analogous one for all the solid solutions. With an increase in the gallium content, the form of the loop is retained, but the magnetization value decreases monotonically. The coercive field also increases and in the sample with x = 0.17 (Cu_2MnBO_5-like phase) it reaches the value of $H_C \approx 4$ kOe, which is four times higher than the Cu_2MnBO_5 value while the magnetization decreases by two times.

The obtained thermal dependences of magnetization (Fig. 3) were analyzed using the modified Curie-Weiss law [3]:

$$\chi = \chi_0 + \frac{C}{T-\theta} \quad (2)$$

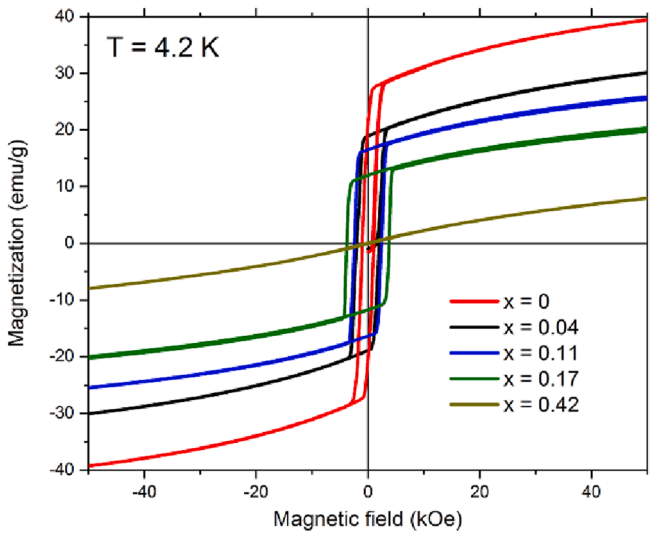

Fig. 6. The field dependences of magnetization of $Cu_2Mn_{1-x}Ga_xBO_5$, obtained at T = 4.2 K, $H||z$. The analogous dependence of parent Cu_2MnBO_5 and $Cu_2Mn_{0.58}Ga_{0.42}BO_5$ (possesses the structure of Cu_2GaBO_5) of the middle concentration range is shown for comparison. The sample $Cu_{1.91}Mn_{0.92}Ga_{0.17}BO_5$ possesses the structure of copper-manganese ludwigite.

As the experimental dependences deviate from the linear law, the temperature-independent contribution χ_0 was specified as a separate term. It consists of the diamagnetic contribution and Van Vleck paramagnetism: $\chi_0 = \chi_d + \chi_{VV}$; C is the Curie constant; θ is the paramagnetic Curie-Weiss temperature. Due to the presence of three fitting parameters

(too many) the approximation did not give reliable results at the initial stage. Therefore, it was necessary to reduce the quantity of the fitting parameters: the temperature-independent term was estimated theoretically and the fitting was done using two parameters, namely, the Curie constant C and the paramagnetic temperature θ. The temperature-independent contribution was estimated in a similar way as in [5]. The obtained results are presented in Table 7.

After reducing the number of the fitting parameters, the dependences of $1/(\chi-\chi_0)(T)$ were plotted and fitted using (2) in the temperature range 170–270 K. The data were analyzed for all the studied samples in three directions of the magnetic field (Fig. S1). Plotting thermal curves of inverse susceptibility allows one to reveal a significant non-monotonically changed anisotropy in the paramagnet phase. Moreover, all the dependences are nonlinear in the paramagnetic phase like in the solid solutions $Cu_2Mn_{1-x}Ga_xBO_5$ of the middle concentration range due to the presence of the short-range correlation above the transition temperature. As a consequence, it is possible to make only the qualitative comparison of the obtained Curie-Weiss temperatures and effective magnetic moments (Table 7). In Table 7 the theoretically calculated effective magnetic moments are presented for comparison for each compound. The calculation was carried out using the expressions:

$$\mu_{eff}^2 = \mu_B^2 \cdot \sum_i N_i \cdot \mu_i^2 \quad (3.1)$$

$$\mu_i^2 = g_i^2 \cdot S \cdot (S+1) \quad (3.2)$$

where i is the type of magnetic ion (Cu^{2+}, Mn^{3+}or Mn^{2+}), N_i is the number of i-type ions in the formula unit in agreement with the actual concentration, g_i is the Lande g-factor of the ions of i-type ($g(Cu^{2+}) = 2.2$ [21], $g(Mn^{3+}) = 2$ [22], $g(Mn^{2+}) = 2$ [22]), S is the spin moment of the i^{th} ion ($S(Cu^{2+}) = 1/2$, $S(Mn^{3+}) = 2$), μ_B is the Bohr magneton. The g-factor value of the Cu^{2+} ion was in agreement with [21] and the value is in good agreement with the experimentally obtained range 2.05–2.27 for Cu_2GaBO_5 and Cu_2AlBO_5 compounds [23].

As one can see in Table 4, the increase in the gallium content in all the samples leads to the enhancement of antiferromagnetic interactions: there is an increase in the value of the negative Curie-Weiss temperature for all the directions. In $Cu_{1.91}Mn_{0.84}Ga_{0.25}BO_5$ with the structure of Cu_2GaBO_5-like phase this value is $\theta(H||x) = -180.9$ K, which is two and a half times higher than the value of the parent gallium ludwigite ($\theta(H\perp z) = -74$ K [21]). A slower increase in the part of antiferromagnetic interactions also occurs in the Cu_2MnBO_5-like phase, in agreement with the tendency of the slope angle of $(\chi\text{-}\chi_0)^{-1}(T)$ to change with the corresponding increase in the modulus of the θ temperatures.

In the paramagnetic phase the dependences of reverse susceptibility of the samples belonging to the Cu_2MnBO_5-like phase are linear only at high temperatures which are caused by the presence of ferrimagnetic interactions in the paramagnetic phase [5]. Therefore, there is some error in the determination of the fitting parameters of the modified Curie-Weiss law for these materials. In turn, the dependences of $Cu_{1.91}Mn_{0.84}Ga_{0.25}BO_5$ which is isostructural to Cu_2GaBO_5 are more linear with a low error in the fitting parameters and determination of effective magnetic moments. For this sample, there is good agreement between the experimental orientational effective magnetic moments and the theoretically expected one (the average value of the experimentally obtained magnetic moment is $5.18\mu_B$, while the theoretically expected one is $5.21\mu_B$). The comparison of the experimental and theoretically calculated effective magnetic moments of other samples which are isostructural to the Cu_2MnBO_5-like phase shows a larger deviation due to the fitting error as a consequence of the insufficiency of the temperature range used [5]. However, a significant anisotropy of the effective magnetic moments was revealed, which can be explained by a large difference of the effective g-factor, depending on the sample orientation. For the parent Cu_2MnBO_5 and Cu_2GaBO_5 ludwigites the values of effective g-factor lie in the ranges 1.87–2.04 and 2.05–2.27, respectively. The notable distortions of the Me-O octahedral in the solid solutions greatly exceeded the ones in pure ludwigites, which can lead to the merge of these value ranges or to a broadening of each of them. Nevertheless, the example of $Cu_{1.91}Mn_{0.84}Ga_{0.25}BO_5$ (in Cu_2GaBO_5-like phase) shows good agreement between the experimentally determined and the theoretically predicted effective magnetic moments upon the accurate determination of composition. Previously, this issue was controversial in analyzing the analogous data for solid solutions of the middle concentration range [5].

As shown earlier [5], the evidence for the spin glass state was found in the samples with large gallium content. This type of magnetic state often occurs even in double (with two types of metal cations) heterometallic ludwigites and it is highly possible in triple ones (three types of metal cations as in the studied compound $Cu_2Mn_{1-x}Ga_xBO_5$). As a rule, the degree of magnetic ordering in ludwigites is determined by the degree of cation ordering over four nonequivalent positions [24]. In parent Cu_2MnBO_5, as shown earlier using neutron diffraction [5], the cations are ordered statistically, three of four positions are occupied by copper, with only one occupied by manganese. However, the magnetic moment of one of the copper position is quite low, which probably indicates the partial ordering due to the frustration of exchange interactions. In Cu_2GaBO_5 only two of four positions are fully occupied by copper cations, being ordered antiferromagnetically. Other two positions are mixed ones (Cu/Ga) and they do not participate in the formation of long-range magnetic ordering, being paramagnetic ones [4]. Upon the Mn → Ga substitution, the changes in the bond lengths in the Me-O octahedra and lattice parameters are minimal in the Cu_2MnBO_5-like phase [6]. The structure of Cu_2MnBO_5 demonstrates extraordinary rigidity regarding the substitution. Thus, one can make a conclusion on the arrangement of trivalent gallium in the position of Mn^{3+} (M4) in this system. But the question on the full or partial magnetic ordering in the studied solid solutions is still open. To completely study the transitional features, the thermal dependences of *ac*-susceptibility of $Cu_2Mn_{1-x}Ga_xBO_5$ were obtained and analyzed.

The thermal dependences of the real and imaginary part of *ac*-susceptibility obtained upon cooling $Cu_{1.8}Mn_{1.16}Ga_{0.04}BO_5$ with the minimum gallium content in the zero *dc* magnetic field are presented in Fig. 7. The anomalies of the *ac*-susceptibility were found in the 70–85 K temperature range both in the real and imaginary parts. Two peaks were found with a strong dependence on the frequency of the alternative field in the real part of susceptibility. The central positions of these peaks correspond to the temperatures of magnetic phase transitions. In the analogous dependences of the imaginary part there is an inflection of the curves which is also related to the phase transition temperatures. The inflection positions also demonstrate a strong dependence on the

Table 4
The Curie-Weiss temperatures and effective magnetic moments of $Cu_2Mn_{1-x}Ga_xBO_5$, obtained by fitting the inverse magnetic susceptibility using the modified Curie-Weiss law. The data are presented for three different directions of the applied magnetic field $H||x$, $H||y$, $H||z$. The theoretically calculated effective magnetic moments are presented for comparison for each compound.

Compound	θ, K $H\|\|z$	θ, K $H\|\|x$	θ, K $H\|\|$y	μ_{eff}, μ_B $H\|\|z$	μ_{eff}, μ_B $H\|\|x$	μ_{eff}, μ_B $H\|\|y$	μ_{eff} - theor, μ_B
$Cu_{1.8}Mn_{1.16}Ga_{0.04}BO_5$	−45.4	−8.9	−39.8	5.07	4.44	5.22	6.00
$Cu_{1.87}Mn_{1.02}Ga_{0.11}BO_5$	−50.4	−41.6	−51.2	4.82	4.59	4.72	5.61
$Cu_{1.91}Mn_{0.92}Ga_{0.17}BO_5$	−60.2	−58.7	−69.5	4.61	3.93	5.57	5.38
$Cu_{1.91}Mn_{0.84}Ga_{0.25}BO_5$	−94.5	−180.9	−75.7	5.06	4.69	5.78	5.21

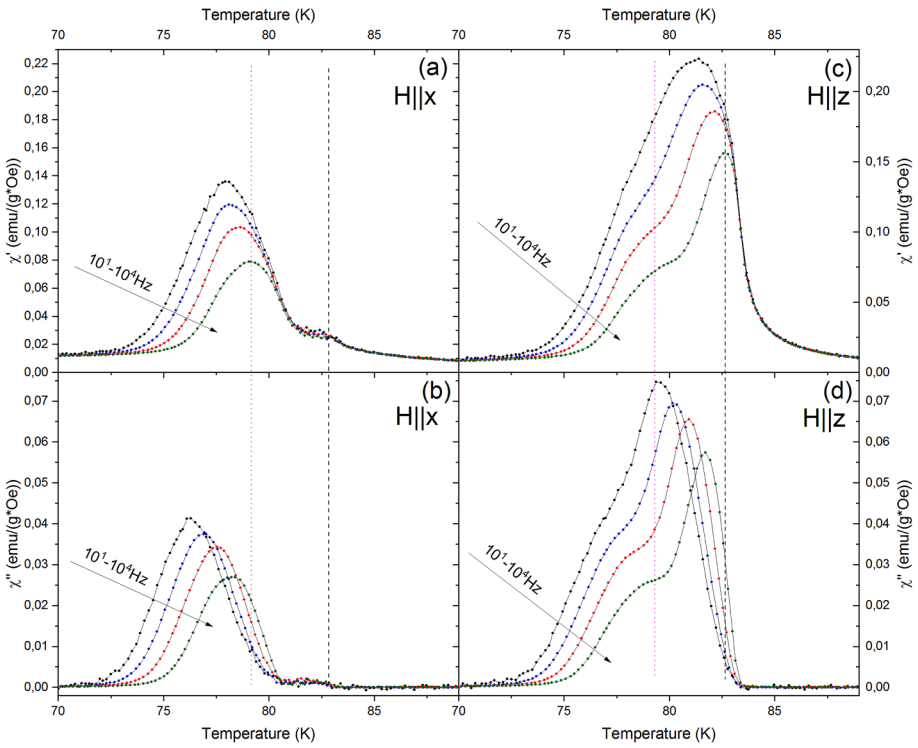

Fig. 7. The thermal dependences of the real and imaginary part of the *ac*-susceptibility obtained under the zero *dc* magnetic field (amplitude 10 Oe) of the sample $Cu_{1.8}Mn_{1.16}Ga_{0.04}BO_5$: (a), (b) – $H||x$; (c), (d) – $H||z$.

frequency. An interesting feature of the obtained curves for this sample is the orientational dependence of the χ' peak value of the high-temperature peak, which is rather intensive at $H||z$ and it almost disappears at $H||x$. At the same time, the value of the low-temperature peak does not depend on the sample orientation. The amplitude stability of the low-temperature phase transition peak and amplitude anisotropy of the high-temperature one indicate different origin of these phase transitions.

Earlier, the strong dependence of the FH-FC hysteresis on the value of the applied magnetic field was found in Cu_2MnBO_5 [3]. Thus, the temperature of this anomaly tends to $T_C = 92$ K (in Cu_2MnBO_5) with a decrease in the magnetic field. Therefore, it can be supposed that the second peak of *ac*-susceptibility of $Cu_{1.8}Mn_{1.16}Ga_{0.04}BO_5$ corresponds to the FH-FC hysteresis anomaly. In this case, the peak position would depend on the value of external magnetic field to a great extent. The measurements of *ac*-susceptibility of the sample upon applying the external *dc* magnetic field $H = 200$ Oe in the direction $H||x$ were made to prove this hypothesis. The results are presented in Fig. 8.

The hypothesis on the involvement of the low-temperature peak of *ac*-susceptibility to FH-FC hysteresis was not confirmed; there is no shift of the peak in the external *dc* magnetic field. In the remaining temperature range down to 4.2 K there are no other anomalies. However, the application of the *dc* magnetic field leads to the splitting of the primary peaks. As a result, there are four peaks in the 72–85 K temperature range (Fig. 8). The peak amplitude upon applying the *dc* field reduces those obtained in the zero *dc* field by three orders of magnitude.

The thermal dependences of *ac*-susceptibility of $Cu_{1.87}Mn_{1.02}Ga_{0.11}BO_5$ are qualitatively similar to the ones obtained for the sample with $x = 0.04$ (Fig. 9). It also contains two peaks (in the zero *dc* magnetic field), but less resolved due to close peak temperatures.

As one can see in Fig. 9, the peak of the real part of *ac*-susceptibility of $Cu_{1.87}Mn_{1.02}Ga_{0.11}BO_5$ indicating the phase transition found in the magnetization measurements is highly asymmetric at low frequencies, which demonstrates the presence of two peak anomalies in this compound. With an increase in the frequency, the peak width significantly decreases and the asymmetry disappears. This can indicate a strong frequency dependence of one of the peaks and weak dependence or its absence for another. Here, the analogous dependences of the imaginary part do not show this asymmetry and can well be described by one profile at a low frequency. This confirms the assumption on the absence of the frequency dependence of one of the peaks, which can correspond to the antiferromagnetic phase transition. It should be noted that the ratio of the peak amplitudes at different sample orientations is in agreement with the thermal magnetization measurements; there is an amplitude difference similar to the magnetization ratio in Fig. 3. Considering the peak intensity ratio of *ac*-susceptibility of $Cu_{1.8}Mn_{1.16}Ga_{0.04}BO_5$ at different sample orientations does not reveal this correspondence: the amplitude of the high-temperature peak sharply decreases disproportionally to the *dc* measurements in the direction $H||x$.

The measurements of *ac*-susceptibility of $Cu_{1.87}Mn_{1.02}Ga_{0.11}BO_5$ were also carried out in the external *dc* magnetic field with the value $H = 200$ Oe in the direction $H||x$ to study the origin of the peaks in detail. The obtained data and their comparison with the dependences in the zero *dc* field are presented in Fig. 10.

The application of the *dc* magnetic field reduces the peak amplitudes and increases the temperature range between the peaks as in the case of the solid solution with the lower gallium content (Fig. 10). Therefore, one can clearly see the presence of two peaks of the real part but only the low-temperature one has a strong frequency dependence. The high-temperature peak does not show this dependence and its position remains constant. This peak is not reflected in the thermal dependence of the imaginary part, which confirms its antiferromagnetic origin: long-range magnetic order in the sites related to this phase transition. The low-temperature peak shows a clear frequency dependence reflecting the time-dependence of phase transition related to it. At high frequencies the temperature of the lower peak is almost the same as the high-temperature one.

Due to the obtained frequency dependent dynamics of the peaks of *ac*-susceptibility in the solid solutions with 0.04 and 0.11 of gallium, the

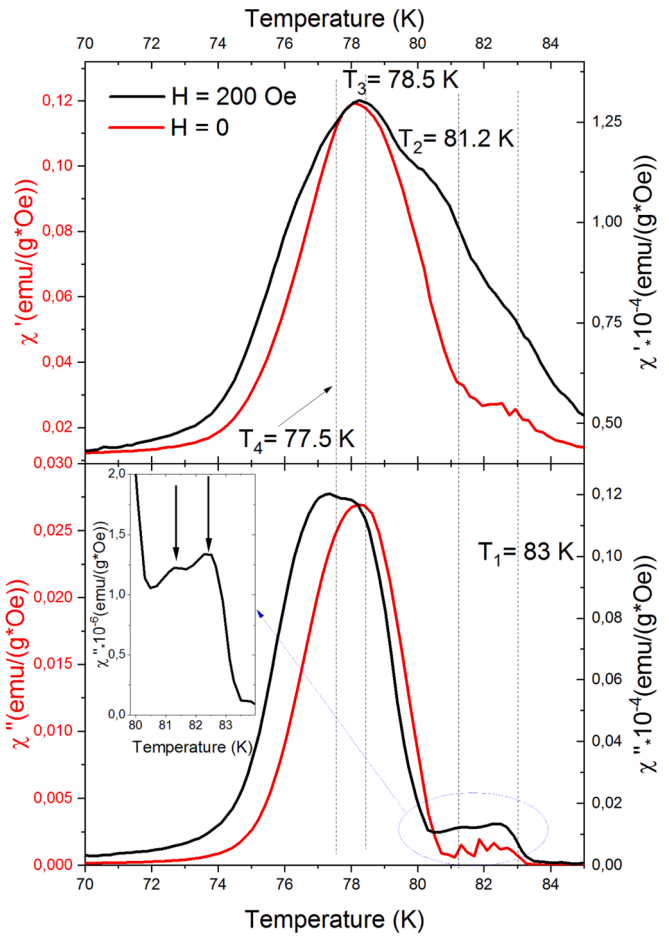

Fig. 8. The thermal dependences of the real and imaginary parts of *ac*-susceptibility (amplitude 10 Oe, $f = 10$ kHz) of $Cu_{1.8}Mn_{1.16}Ga_{0.04}BO_5$ in the zero external magnetic field and in the external *dc* magnetic field $H = 200$ Oe in the direction $H||x$.

Mydosh parameter indicating the presence or absence of the spin glass behavior was estimated for each direction of the magnetic field [25]:

$$\Omega = \frac{T_2 - T_1}{T_2 \cdot (\log\nu_2 - \log\nu_1)}; \quad (4)$$

where T_1 and T_2 are the temperatures of the peak center corresponding to frequencies ν_1 and ν_2; the frequencies were obtained by fitting with the help of the Gauss function of the experimental thermal dependences of the real part of *ac*-susceptibility for each sample. For the sample with $x = 0.04$ two peaks were analyzed, which were clearly indicated in the absence of the external *dc* magnetic field. For this sample, the Mydosh parameter was not calculated upon applying the $H = 200$ Oe *dc* field due to the low resolution of the obtained peaks and large fitting error, as a consequence. The calculated values of the Mydosh parameter corresponding to each peak of the studied solid solutions with $x = 0.04$ and $x = 0.11$ are presented in Table 5.

It is known [26] that the typical values of the Mydosh parameter for canonical spin glass systems are in the range from 0.004 to 0.02. Spin glasses with higher values are characterized as cluster spin glass systems [27]. As one can see from Table 4, the Mydosh parameters are different at different orientations of the sample for both solid solutions. The highest values (at the lower boundary of the identification of the canonical spin glasses) characterize the low-temperature phase transition T_2 for both compounds and reach the value of 0.0098. The analogous values of the Mydosh parameter of the solid solutions $Cu_2Mn_{1-x}Ga_xBO_5$ of the middle concentration range [5] amount to 0.0287, which to a great extent exceeds the results obtained in this work. This means that the part of the spin glass state in the samples with the low gallium content with the structure of Cu_2MnBO_5 is much smaller than in the samples of Cu_2GaBO_5-like phase with the comparable content of Mn/Ga. The Mydosh parameter of the high-temperature phase transition T_1 of the solid solution $Cu_{1.87}Mn_{1.02}Ga_{0.11}BO_5$ does not exceed 0.0015, which confirms the assumption on its long-range origin. The absence of anomalies in $\chi''(T)$ in this temperature range allows one to identify this phase transition as a transition of a part of the cation positions to the antiferromagnetic state. At the low-temperature phase transition, a part of the magnetic moments does not order and in the low-temperature phase there is a spin glass state in agreement with the obtained Mydosh parameter. Applying the *dc* magnetic field reduces the part of the disordered magnetic moments.

In the compound with $x = 0.04$ both phase transitions can reflect the transition of a part of magnetic moments to the spin glass state. However, in this compound there is a significant anisotropy and almost full damping of the high-temperature peak in the direction of $H_{ac}||x$. This reduces the accuracy of determining the center position (taking into account the fitting) due to a large width and weak intensity.

The thermal dependences of *ac*-susceptibility of the samples with higher gallium content ($x = 0.17$ (at this concentration in the flux the system shows phase separation, two samples were selected: one with the Cu_2GaBO_5-like phase properties, and another one possessing the high-temperature phase transition inherited from the Cu_2MnBO_5 phase) and $x = 0.25$ (the compound having the properties of both phases and the Cu_2GaBO_5-like structure) were obtained at two orientations of the sample $H_{ac}||x$ and $H_{ac}||z$, at $H_{dc} = 0$. The obtained curves are presented in Figs. 11 and 12.

As one can see in Figs. 11 and 12, the thermal dependences of *ac*-susceptibility of these samples are similar to each other: each of them demonstrates a high-temperature peak corresponding to the Cu_2MnBO_5-like phase despite the structure of the Cu_2GaBO_5-like phase. Evidently, the presence of this phase transition is caused by Mn-containing subsystem ordering. However, the jump in *dc* magnetization is weakly expressed at these temperatures. The earlier studied change in the symmetry of the Me-O octahedra showed the difference of $<$ M3-O $>$ for $x = 0.25$ from that for Cu_2GaBO_5. The octahedron represents a bipyramid with elongated bonds of 2.267 Å, the other bonds have the length close to 2.00 Å. This distortion type is very close to M4 position in Cu_2MnBO_5 occupied by Mn^{3+}.Thus, it can be concluded that the positions M3 and M4 in the compounds with $x = 0.17$ and $x = 0.25$ are occupied by manganese cations with different probability and the phase transition inherited from the Cu_2MnBO_5-like phase is close to ferrimagnetic with the antiferromagnetic arrangement of the Mn^{3+} moments in these positions.

Besides the high-temperature peak, in the samples with $x = 0.17$ and $x = 0.25$ there are anomalies in the low-temperature range in the form of a broad asymmetric peak with the center at about 20 K corresponding phase transition inherited from Cu_2GaBO_5. This low-temperature peak can not be described by one profile, as it consists of two profiles: the broad and the narrow one. The positions of the centers of these profiles were estimated by fitting with the help of the Gauss function for each frequency value. An interesting feature of the *ac*-susceptibility of both samples is the difference in the intensity ratios of the high-temperature and low-temperature peaks: for the sample with $x = 0.25$ the intensities are almost equal, for the sample with $x = 0.17$ the intensity of the high-temperature peak is several times lower. It can be caused by the suppression of this ferrimagnetic transition in the Cu_2GaBO_5-like phase and redistribution of the cations over non-equivalent positions.

The obtained curves of $Cu_{1.91}Mn_{0.84}Ga_{0.25}BO_5$ at different sample orientations show almost no differences in the whole temperature range; there is no anisotropy (Fig. 11). But the pronounced anisotropy of the low-temperature peaks is reflected in the obtained curves of $Cu_{1.91}Mn_{0.92}Ga_{0.17}BO_5$ (the high-temperature peak does not depend on

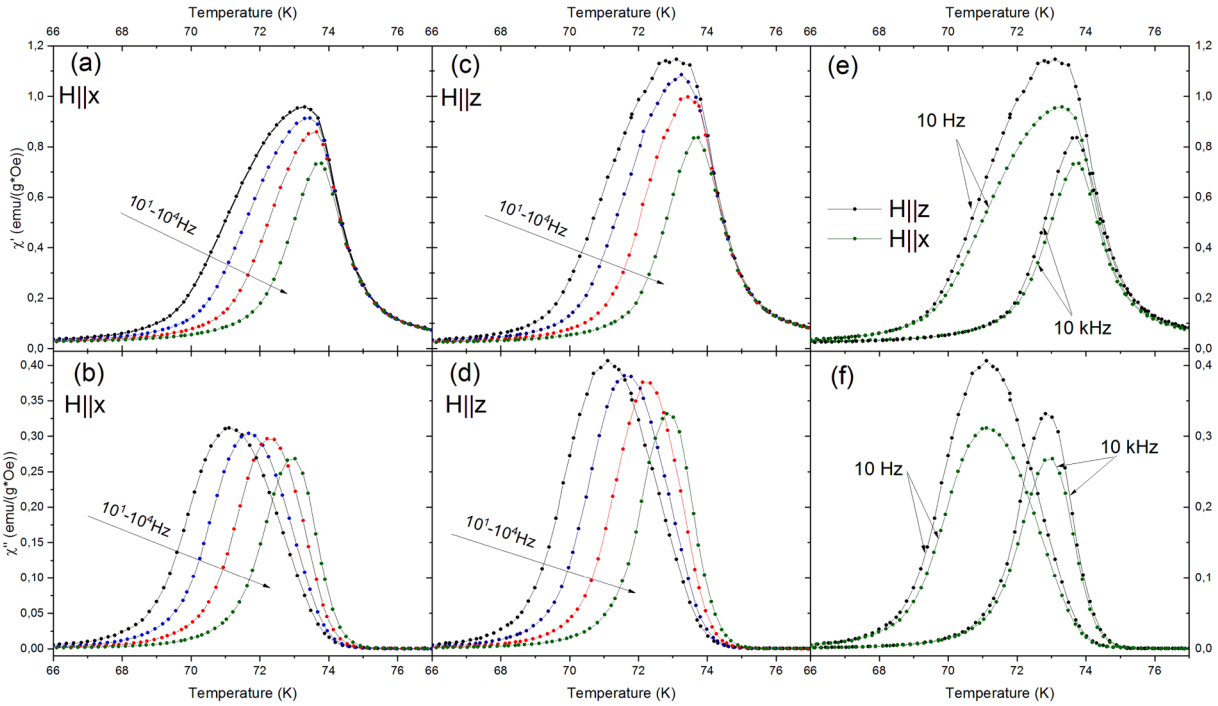

Fig. 9. The thermal dependences of the real and imaginary parts of *ac*-susceptibility obtained in the zero *dc* magnetic field (amplitude 10 Oe) of $Cu_{1.87}Mn_{1.02}Ga_{0.11}BO_5$: (a), (b) $H||x$; (c), (d) $H||z$; (e), (f) the comparison of the dependences obtained at $H||x$ and $H||z$ at 10 Hz and 10 kHz.

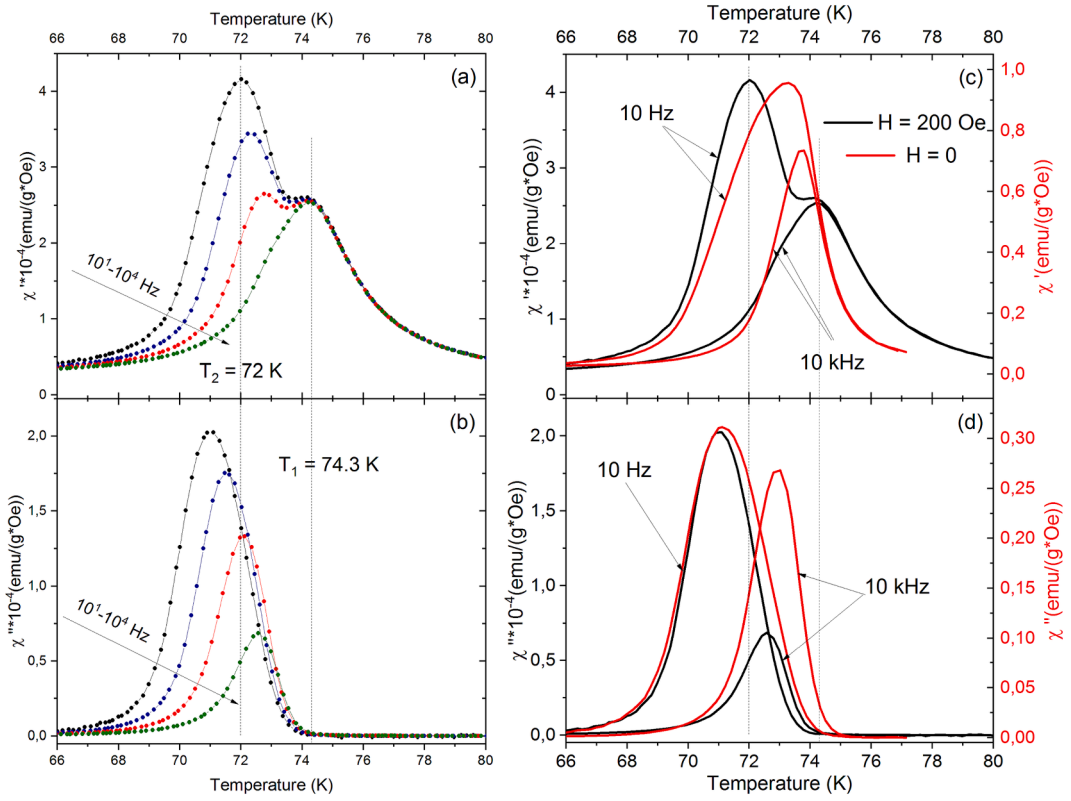

Fig. 10. The thermal dependences of the real and imaginary part of *ac*-susceptibility (amplitude 10 Oe, $f = 10$ Hz, 10 kHz) of $Cu_{1.87}Mn_{1.02}Ga_{0.11}BO_5$ in the zero magnetic field and in the external *dc* magnetic field $H = 200$ Oe in the direction $H||x$. (a), (c) real part of the *ac*-susceptibility; (b), (d) imaginary part of the *ac*-susceptibility. (a), (b) dependences obtained in the external magnetic field $H = 200$ Oe at frequencies 10–10^4 Hz; (c), (d) comparison of the dependences obtained in the field $H = 200$ Oe and without any field for the frequencies 10 Hz and 10 kHz.

Table 5
The Mydosh parameters of the solid solutions with $x = 0.04$ and $x = 0.11$ calculated from the dependences of *ac*-susceptibility obtained at $H_{ac}||z$ and $H_{ac}||x$, at $H_{dc} = 0$ and $H_{dc} = 200$ Oe. T_{C1}, T_{C2} are the central positions of the peaks in the thermal dependences of the real part of *ac*-susceptibility corresponding to the phase transitions.

Compound	Ω, $H_{ac}||z$ $H_{dc} = 0$		Ω, $H_{ac}||x$ $H_{dc} = 0$		Ω, $H_{ac}||x$ $H_{dc} = 200$Oe	
$Cu_{1.8}Mn_{1.16}Ga_{0.04}BO_5$	T_{C1}	T_{C2}	T_{C1}	T_{C2}		
	80–81.7 K	77–79.1 K	82.8–83.1 K	78–79 K		
	0.0075	0.009	0.0009	0.0042		
$Cu_{1.87}Mn_{1.02}Ga_{0.11}BO_5$	T_{C1}	T_{C2}	T_{C1}	T_{C2}	T_{C1}	T_{C2}
	73.4–73.7 K	71.6–73.6 K	73.5–73.7 K	71.8–73.3 K	74.4–74.5 K	71.8–73.1 K
	0.0011	0.0093	0.0015	0.0098	0.0007	0.0059

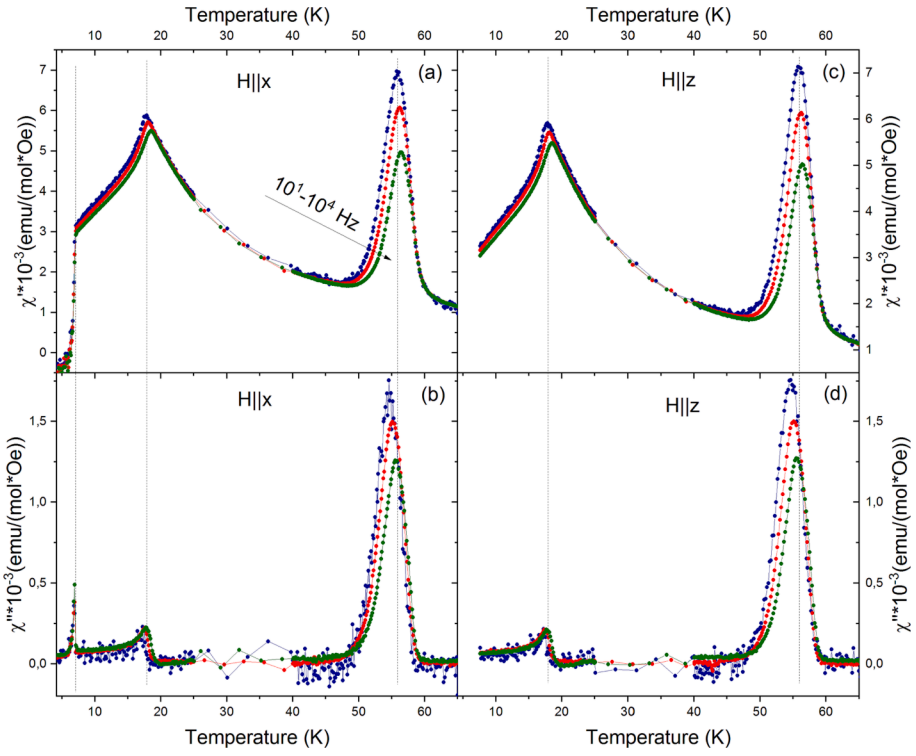

Fig. 11. The thermal dependences of the real and imaginary part of *ac*-susceptibility obtained in the zero *dc* magnetic field (10 Oe) of $Cu_{1.91}Mn_{0.84}Ga_{0.25}BO_5$: (a), (b) – $H||x$; (c), (d) – $H||z$.

the orientation): the position of the center of the narrow peak does not depend on the sample orientation, but the broad one changes its position noticeably shifting to the low-temperature range at $H||x$.

For these compounds the Mydosh parameters were also calculated. The obtained results are presented in Table 6.

As one can see from Table 6, the high-temperature phase transition in both samples is characterized by the low Mydosh parameter values, implying the low part of the statistically disordered "freezed" magnetic moments. The Mydosh parameters of the low-temperature peaks for both samples are the marginal values between the canonical and cluster spin glasses and they are similar to analogous values for the studied solid solutions of the middle concentration range [5]. The low value of the Mydosh parameter (0.028) for T_{C2} of the compound with $x = 0.25$ is caused by a significant error in the determination of the peak center position due to its large width.

5. Conclusions

The magnetic properties of the $Cu_2Mn_{1-x}Ga_xBO_5$ solid solutions with a high manganese concentration are studied in detail near the concentration Cu_2MnBO_5/Cu_2GaBO_5 phase boundary following the study of its structure evolution [6]. Using X-ray absorption spectroscopy, the chemical and valence composition of the samples were determined with a high accuracy. The presence of a small fraction of Mn^{2+} along with copper cations in the bivalent subsystem was shown. The obtained orientational thermal dependences of magnetization revealed a non-monotonic change of magnetization relative to the gallium content within the copper-manganese ludwigite phase, indicating different position distribution in the samples with different composition. This manifests the ambiguity of the gallium distribution over four nonequivalent positions of the unit cell. The presented first-principle calculations of the energy of the parent ludwigite structures with different cationic distribution confirmed the preference of the configurations with several gallium positions and manganese cation ordering at position 4.

A complex pattern of magnetic phase transitions was found in the compounds with $x = 0.17$–0.25 of gallium belonging the concentration phase boundary. These samples undergo several magnetic phase transitions inherited from both parent phases. The thermal dependences of the *ac* magnetic susceptibility in the zero and nonzero *dc* magnetic field were studied for a more detailed investigation of these phase transitions. The splitting of the peak of the real part of *ac*-susceptibility of the high-

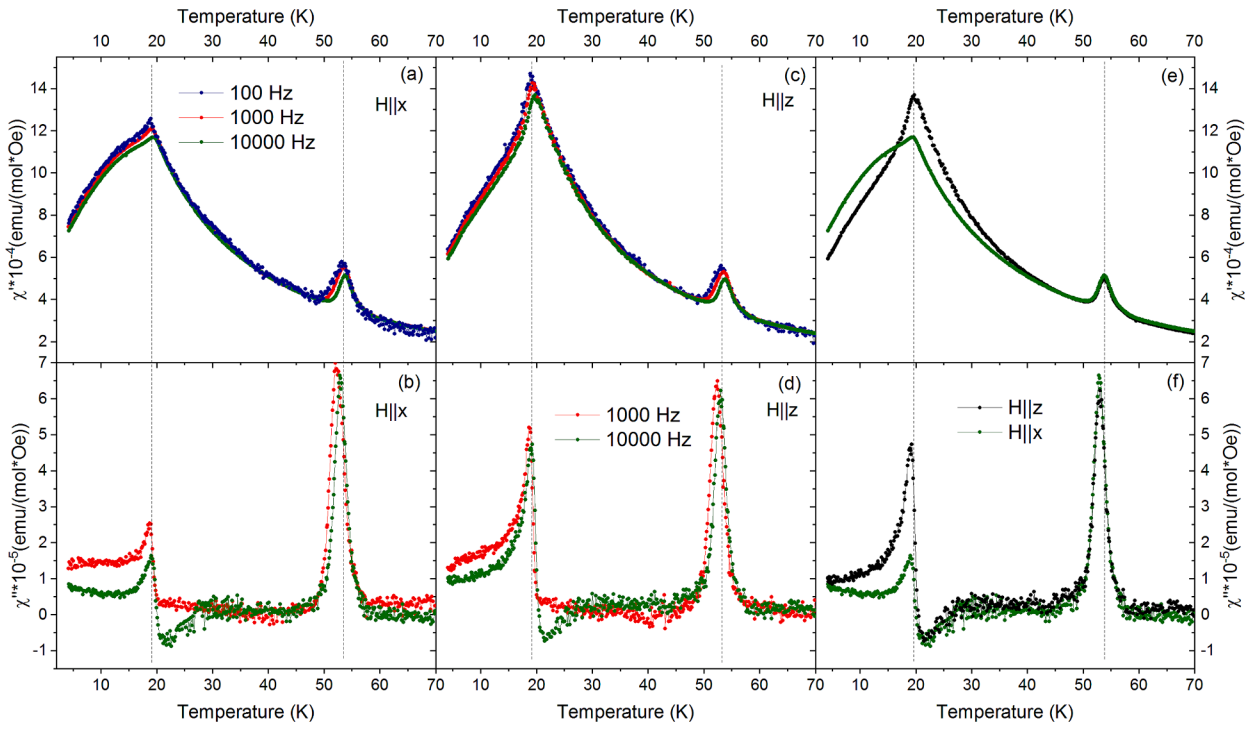

Fig. 12. The thermal dependences of the real and imaginary part of *ac*-susceptibility obtained in the zero *dc* magnetic field (10 Oe) of $Cu_{1.91}Mn_{0.92}Ga_{0.17}BO_5$ (isostructural to the Cu_2GaBO_5-like phase): (a), (b) $H||x$; (c), (d) $H||z$; (e), (f) the comparison of the dependences obtained at different sample orientation at $\nu = 10$ kHz. The data for 100 Hz are not presented for the imaginary part due to the weak signal.

Table 6
The Mydosh parameters of $Cu_{1.91}Mn_{0.92}Ga_{0.17}BO_5$ and $Cu_{1.91}Mn_{0.84}Ga_{0.25}BO_5$, calculated from the dependences of *ac*-susceptibility obtained at $H_{ac}||x$ and $H_{ac}||z$, at $H_{dc} = 0$. T_{C1}, T_{C2}, T_{C3} are the central positions of the peaks of the real part corresponding to the phase transitions.

Compound	Ω, $H_{ac}\|\|z$			Ω, $H_{ac}\|\|x$		
$Cu_{1.91}Mn_{0.92}Ga_{0.17}BO_5$	T_{C1}	T_{C2}	T_{C3}	T_{C1}	T_{C2}	T_{C3}
	53.4–53.8 K	19.9–20.5 K	19.3–19.9 K	53.5–53.8 K	19.0–19.7 K	16.3–16.35 K
	0.0037	0.0166	0.0174	0.0026	0.0175	0.0021
$Cu_{1.91}Mn_{0.84}Ga_{0.25}BO_5$	T_{C1}	T_{C2}	T_{C3}	T_{C1}	T_{C2}	T_{C3}
	55.9–56.4 K	19.7–19.8 K	17.9–18.6 K	55.9–56.4 K	18.5–19.1 K	17.9–18.6 K
	0.0044	0.0028	0.0198	0.0044	0.0177	0.0209

temperature phase transition in the Cu_2MnBO_5-like phase at different frequencies and the orientational dependence was already found in the nonzero *dc* magnetic field. The observed effect was significantly enhanced by applying the *dc* magnetic field. The Laue method confirms the quality and homogeneity (no disoriented domains) of the studied crystal samples excluding the influence of differently oriented magnetic directions at the phase transition temperature. The peak of the low-temperature magnetic phase transition inherited from Cu_2GaBO_5 also has a complex form in the thermal curves of *ac*-susceptibility and consists of two maxima of different origin. The multiplicity of the magnetic phase transitions both in the Cu_2MnBO_5-like phase and in the Cu_2GaBO_5-like phase can be associated with the consistent ordering of the magnetic moments in different magnetic subsystems formed from the nonequivalent cation positions. The calculated Mydosh parameters for the observed phase transitions reveal a long-range character of the high-temperature transitions for each compound and the presence of a fraction of "freezed" spin moments, i.e. the presence of the spin glass state.

CRediT authorship contribution statement

Evgeniya Moshkina: Conceptualization, Methodology, Investigation, Writing – original draft, Writing – review & editing, Visualization. **Evgeniy Eremin:** Investigation, Resources, Writing – review & editing. **Alexey Veligzhanin:** Investigation, Resources, Writing – review & editing. **Maksim Pavlovskiy:** Investigation, Resources. **Svetlana Sofronova:** Investigation, Writing – review & editing. **Veronika Titova:** Investigation. **Leonard Bezmaternykh:** Conceptualization, Supervision.

Declaration of Competing Interest

The authors declare that they have no known competing financial interests or personal relationships that could have appeared to influence the work reported in this paper.

Data availability

No data was used for the research described in the article.

Acknowledgements

The work was carried out within the state assignment of Kirensky Institute of Physics. The magnetic measurements were obtained on the analytical equipment of the Krasnoyarsk Regional Center of Research Equipment of the Federal Research Center "Krasnoyarsk Science Center

SB RAS".

Appendix A. Supplementary data

Supplementary data to this article can be found online at https://doi.org/10.1016/j.jmmm.2023.171072.

References

[1] E.M. Moshkina, N.A. Belskaya, M.S. Molokeev, A.F. Bovina, K.A. Shabanova, D. Kokh, Y.V. Seretkin, D.A. Velikanov, E.V. Eremin, A.S. Krylov, L. N. Bezmaternykh, Growth Conditions and the Structural and Magnetic Properties of Cu_2MBO_5 (M = Cu, Fe, Mn) Oxyborates with a Ludwigite Structure, J. Exp. Theor. Phys. 136 (1) (2023) 17–25.

[2] S. Sofronova, E. Moshkina, I. Nazarenko, Y.u. Seryotkin, S.A. Nepijko, V. Ksenofontov, K. Medjanik, A. Veligzhanin, L. Bezmaternykh, Crystal growth, structure, magnetic properties and theoretical exchange interaction calculations of Cu_2MnBO_5, Journal of Magnetism and Magnetic Materials. – 420 (2016) 309–316.

[3] E. Moshkina, C. Ritter, E. Eremin, S. Sofronova, A. Kartashev, A. Dubrovskiy, L. Bezmaternykh, Magnetic structure of Cu_2MnBO_5 ludwigite: thermodynamic, magnetic properties and neutron diffraction study, J. Phys.: Condens. Matter. 29 (2017), 245801.

[4] A.A. Kulbakov, R. Sarkar, O. Janson, S. Dengre, T. Weinhold, E.M. Moshkina, P. Y. Portnichenko, H. Luetkens, F. Yokaichiya, A.S. Sukhanov, R.M. Eremina, P. h. Schlender, A. Schneidewind, H.-H. Klauss, D.S. Inosov, Destruction of long-range magnetic order in an external magnetic field and the associated spin dynamics in Cu_2GaBO_5 and Cu_2AlBO_5 ludwigites, Phys. Rev. B 103 (2021), 024447.

[5] E. Moshkina, E. Eremin, D. Velikanov, A. Bovina, M. Molokeev, Y. Seryotkin, M. Cherosov, R. Batulin, I. Nemtsev, L. Bezmaternykh, Structural and magnetic alteration of Cu_2GaBO_5 forced by Mn^{3+} doping, J. Alloys Compd. 902 (2022), 163822.

[6] E. Moshkina, A. Krylov, D. Kokh, K. Shabanova, M. Molokeev, A. Bovina, M. Plyaskin, N. Rostovtsev, L. Bezmaternykh, Multicomponent flux growth and composition control of Cu_2MnBO_5: Ga ludwigites, CrystEngComm 24 (2022) 3565.

[7] A.A. Chernyshov, A.A. Veligzhanin, Y.V. Zubavichus, Nuclear Instrum. Methods Phys. Res. Section A: Accel. Spectrom. Detect. Assoc. Equip. 603 (2009) 95–98.

[8] M. Newville, J. Synchrotron Radiat. 8 (2001) 322–324.

[9] B. Ravel, M. Newville, J. Synchrotron Radiat. 12 (2005) 537–541.

[10] P. Blaha, K. Schwarz, G. Madsen, D. Kvasnicka, J. Luitz, An Augmented Plane Wave + Local Orbitals Program for Calculating Crystal Properties, Vienna University of Technology Inst. of Physical and Theoretical Chemistry, Vienna, 2015.

[11] P. Blaha, K. Schwarz, F. Tran, R. Laskowski, G. Madsen и L. Marks, WIEN2k: An APW+lo program for calculating the properties of solids, J. Chem. Phys. -2020 - vol. 152 - p. 074101.

[12] E. Sjöstedt, L. Nordström, D.J. Singh, An alternative way of linearizing the augmented plane-wave method, Solid State Communications 114 (1) (2000) 15–20.

[13] J.P. Perdew, Y. Wang, Accurate and simple analytic representation of the electron-gas correlation energy, Phys. Rev. B 45 (23) (1992) 13244–13249.

[14] J.P. Perdew, K. Burke, M. Ernzerhof, Generalized Gradient Approximation Made Simple, Phys. Rev. Lett. 77 (18) (1996) 3865–3868.

[15] V.I. Anisimov, J. Zaanen, O.K. Andersen, Band theory and Mott insulators: Hubbard U instead of Stoner I, Phys. Rev. B 44 (3) (1991) 943–954.

[16] P.E. Blöchl, O. Jepsen, O.K. Andersen, Improved tetrahedron method for Brillouin-zone integrations, Phys. Rev. B 49 (23) (1994) 16223–16233.

[17] J.H. Hubbell and S.M. Seltzer. X-Ray Mass Attenuation Coefficients, NIST Standard Reference Database 126 (2004).

[18] M. Debnath, E. Bose, S. Pal, Impact of non-magnetic Zn^{2+} doping on the structural, magnetic and magnetocaloric properties of $Nd_{0.5}Ca_{0.5}Mn_{1-x}Zn_xO_3$ (x = 0, 0.05, 0.10) compounds, J. Magn. Magn. Mater. 575 (2023), 170752.

[19] Chikazumi, S. Physics of Ferromagnetism / S.Chikazumi. –New York: Oxford University Press, 1997. –Chapters 15-17.

[20] E.E. Bragg, M.S. Seehra, Magnetic Susceptibility of MnF, near T and Fisher's Relation, Phys. Rev. B V. 7, is. 9 (1973) 4197–4202.

[21] R.M. Eremina, T.P. Gavrilova, E.M. Moshkina, I.F. Gilmutdinov, R.G. Batulin, V. V. Gurzhiy, V. Grinenko, D.S. Inosov, Structure, magnetic and thermodynamic properties of heterometallic ludwigites: Cu_2GaBO_5 and Cu_2AlBO_5, J. Magn. Magn. Mater. 515 (2020) 167262.

[22] D.V. Popov, T.P. Gavrilova, I.F. Gilmutdinov, M.A. Cherosov, V.A. Shustov, E. M. Moshkina, L.N. Bezmaternykh, R.M. Eremina, Magnetic properties of ludwigite $Mn_{2.25}Co_{0.75}BO_5$, Journal of Physics and Chemistry of Solids 148 (2021) 10969.

[23] Svetlana Sofronova, Rushana Eremina, Ivan Yatsyk, Evgeniya Moshkina. Exchange Interactions in Cu_2AlBO_5 and Cu_2GaBO_5. AIP Conference Proceedings 2218, 040001 (2020).

[24] S. Sofronova, I. Nazarenko. Ludwigites: From natural mineral to modern solid solutions, Crystal Res. Technol. (2017) 52 (4) 1600338.

[25] S. Ghosh, D.C. Joshi, P. Pramanik, S.K. Jena, S. Pittala, T. Sarkar, M.S. Seehra, S. Thota, Antiferromagnetism, spin-glass state, H-T phase diagram, and inverse magnetocaloric effect in Co_2RuO_4, J. Phys.: Condens. Matter 32 (48) (2020) 485806.

[26] V. Tapati Sarkar, V. Pralong, B.R. Caignaert, Competition between Ferrimagnetism and Magnetic Frustration in Zinc Substituted $YBaFe_4O_7$, Chem. Mater. 22 (2010) 2885–2891.

[27] C.A.M. Mulder, A.J. van Duynevelt, J.A. Mydosh, Susceptibility of the CuMn spin-glass: Frequency and field dependencies, Phys. Rev. B 23 (3) (1981) 1384–1396.